4.2 STRUCTURE OF MERIDIONAL MOISTURE TRANSPORT OVER THE US SOUTHERN GREAT PLAINS OBSERVED BY CO-DEPLOYED AIRBORNE WIND AND WATER VAPOR LIDARS

R. Michael Hardesty[1,2*], Wm. Alan Brewer[1], Christoph J. Senff[2], Brandi J. McCarty[2], Gerhard Ehret[3], Andreas Fix[3], Christoph Kiemle[3], and Edward I. Tollerud[1]

[1]NOAA Earth System Research Laboratory, Boulder, Colorado

[2]Cooperative Institute for Research in Environmental Sciences, University of Colorado at Boulder, Boulder, Colorado

[3]Deutsche Zentrum für Luft- und Raumfahrt (DLR), Oberpfaffenhofen, Germany

1. INTRODUCTION

Moisture transported by the low level jet (LLJ) from the Gulf of Mexico into the Central Great Plains can be nearly significantly higher when compared to periods when a LLJ is not present. LLJ moisture transport plays a role in the development of Mesoscale-Convective Complexes, which provide a significant portion of overall Central Plains precipitation.

Structure and amount of moisture transport by the low level jet at small scales is not easily observed. Both radiosonde and profiler networks provide inadequate temporal and/or spatial resolution to describe wind or moisture gradients with sufficient precision. Aircraft deployment of dropsondes as part of focused field studies improves horizontal resolution, but the expense of deploying large numbers of dropsondes precludes detailed measurements at high spatial resolution.

During the International H_2O Project (IHOP) we applied a remote sensing approach to obtain high resolution moisture transport observations. A Doppler lidar and Differential Absorption Lidar (DIAL) were co-deployed on a Falcon research aircraft to demonstrate the feasibility of the measurements and observe the small-scale structure of moisture transport by the low level jet. The lidar-derived measurements were compared with those from dropsondes to investigate to determine what, if any, important characteristics of LLJ structure might be missed by sampling at the multiple tens-of-km resolution of the dropsonde measurements.

2. MEASUREMENT OVERVIEW

The novel aspect of the IHOP Falcon observation package was the co-deployment of the NOAA Doppler lidar and DLR DIAL instruments on a single aircraft and the subsequent combined analysis of the data streams from the two systems, as originally discussed by Kiemle et al (2007). Prior to IHOP, the DLR DIAL instrument had previously been deployed on the Falcon on a number of occasions to measure atmospheric water vapor (e.g., Ehret, 1999), however IHOP marked the first instance of installation of a second lidar in the cabin.

In preparation for IHOP, the NOAA HRDL system (Grund et al, 2001) was redesigned to fit into the limited space available in the Falcon cabin. The HRDL instrument provides high resolution (30m) measurements of radial wind speed and aerosol backscatter in the lower troposphere. For IHOP, the lidar was mounted in the center aisle of the aircraft such that the laser beam exited the transmitter parallel to the aircraft floor in the forward longitudinal direction. A turning mirror directed the beam into the atmosphere through an aircraft nadir port located just aft of the nadir port through which the DIAL beam was directed.

Throughout IHOP the DLR DIAL system was deployed in a nadir-looking configuration with the beam directed downward through a forward hatch on the Falcon, providing vertical profiles of water vapor below the aircraft. The HRDL system, however, was operated in two different beam configurations for vertical and horizontal wind measurements during the IHOP deployment. Doppler lidar measurements of vertical wind were combined with the DIAL observations to estimate moisture flux profiles, as described by Kiemle et al (2007). For the horizontal moisture transport measurements described here, a conical wedge scanner was inserted into the optical path just inside the aircraft exit port. This scanner deflected the beam 20 degrees from nadir (referenced in aircraft coordinates) and was capable of either continuous or stop-start operation to provide a full conical scan. During IHOP our original intention was to direct the beam in two or more different azimuth directions to estimate the full horizontal

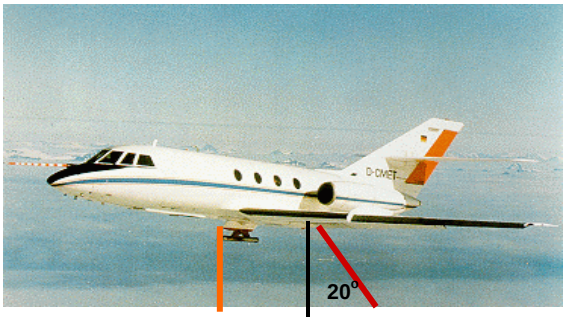

Figure 1: DLR Falcon employed during IHOP indicating nadir DIAL beam (orange) and Doppler beam (red), directed at 20 degree nadir angle transverse to the flight direction.

wind vector. However, a very tight schedule (less than 2 weeks) for installing HRDL on the Falcon precluded full development and testing of hardware and software elements needed to remove the effects of aircraft motion from the lidar-measured wind velocity estimate. As a result, immediately prior to the experiment we elected to fix the scanner azimuth such that the beam was always directed transverse to the aircraft. Fixing the beam direction orthogonal to the aircraft motion vector eliminated the need to actively monitor aircraft velocity and orientation to account for the effects of aircraft forward velocity. Because the aircraft velocity vector could vary slightly from the longitudinal axis of the aircraft because of aircraft yaw, during post-processing we used the high signal-to-noise ratio return from the surface to adjust the measured velocity for aircraft yaw angle variations. The measured velocity of the surface return was subtracted from the computed wind velocity at each range gate.

In addition to the simplicity engendered by fixing the azimuth angle transverse to the aircraft, our rationale for adopting this configuration was based on the typical north-south orientation of the low level jet axis over the Central Great Plains. For the two low-level jet cases studied during IHOP, flight plans were developed that included east-west transects at different latitudes, designed so that the lidar radial velocity vector was directed directly along a north-south orientation. As will be seen in Section 3, these flight tracks captured most, but not all, of the lower troposphere wind motion during the cases studied, especially in the lower troposphere where much of the moisture transport occurred.

2.1 DOPPLER LIDAR

The NOAA HRDL instrument was specifically designed for high resolution probing of the lower

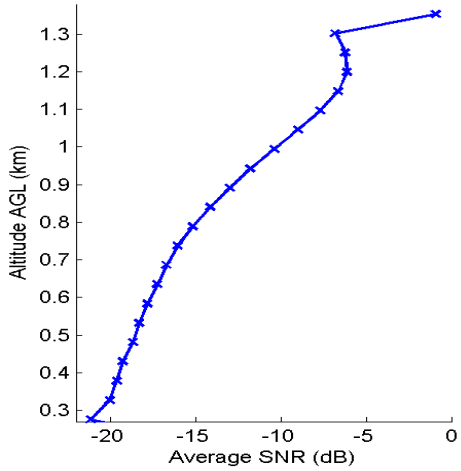

Figure 2: Signal to noise ratio of lidar returns near the ground.

atmosphere. System parameters for the instrument are given in Table 1. Maximum range of the lidar is typically from 3-8 km, depending on aerosol loading. The low pulse energy, high pulse-rate design necessitates averaging of multiple pulses to reduce the noise in the single shot radial velocity estimates, especially near the surface where signal levels are low. For the IHOP moisture transport measurements, data were averaged to 10-s resolution. Figure 2 shows the average wideband carrier to noise ratio (CNR) as a function of altitude measured near the surface during the IHOP flights of June 9, which were typical of the general experiment campaign. It can be seen that CNR ranges from about -5 dB to nearly -20 dB. The impact of low CNR is seen in Figure 3, which shows the instrument

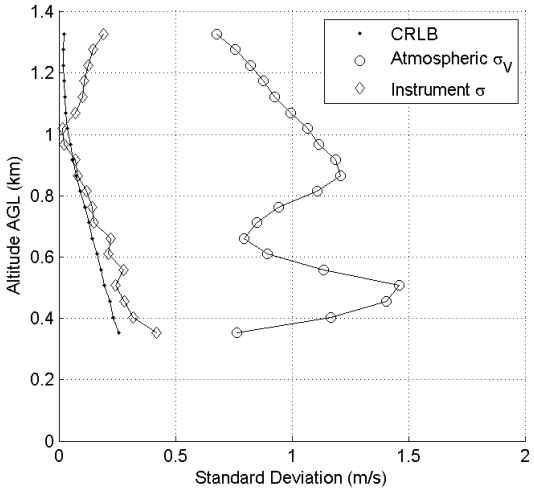

Figure 3: Standard deviation of radial wind estimate due to instrument error and atmospheric effect. Also shown is the Cramer-Rao lower bound (Courtesy Sara Tucker, CIRES).

Table 1: DIAL and HRDL system parameters

Parameter	DIAL	HRDL
Transmitter Type	OPO	Injection seeded solid state
Wavelength (nm)	927	2020
Pulse energy (mJ)	12	2
PRF (Hz)	100	200
Pulse Length (ns)	7	200
Detection	Direct	Heterodyne
Detector type	APD	PIN diode
Telescope diameter (cm)	35	11

measurement error (uncorrelated measurement standard deviation) and the estimated atmospheric variability (correlated measurement standard deviation) in the radial velocity estimate for a portion of the June 9 flight. Standard deviations are computed using an autocovariance technique. The line-of-sight measurement error is generally below about 0.5 m s^{-1} even for these low signal levels until about 400 m altitude, below which the error increases to nearly 2 m s^{-1} in the lowest 400 m. Errors are typically lower at higher altitudes, where signal is generally stronger. Also plotted in Figure 3 is the Cramer-Rao lower bound (minimum error) estimated from the system characteristics.

2.2 DIFFERENTIAL ABSORPTION LIDAR

The DIAL system employed on the Falcon by DLR during IHOP operates in the 920-950 nm range with average output power of 1.8 W, as described in Ehret (1997). In addition to the DIAL measurements, polarization-sensitive backscatter observations at 1064 and 532 nm are obtained. The system can make water vapor measurements in both the stratosphere and troposphere depending on strength of the absorbing line chosen. Because the summer Central Great Plains are characterized by high moisture, a weak line at 926.874 nm was selected for the IHOP measurements. System parameters for the DLR DIAL system are summarized in Table 2.

For IHOP, the online and offline profiles were accumulated to 1-s averaged before applying the DIAL equation, which was run at a vertical resolution of 150 m. The 1-s estimates, characterized by an uncertainty of about 7% (Kiemle et al, 2007), were averaged for 10 s to match the spatial resolution of the wind lidar.

3.0 THE JUNE 9, 2002 CASE

The best case for examining the low level jet was a flight on the morning of June 9, when forecast models had predicted a reasonably strong low level jet and significant moisture transport from the south into Kansas and Nebraska. A flight track was developed designed to measure the moisture into and out of a 285 km square centered just west of Garden City Kansas. Because the models showed meridional flow, the flight track was oriented directly east-west and north south. Figure 4 shows the flight pattern, with color indicating the wind speed measured at a height of 2 km ASL. The region of highest wind speed, as indicated by the red color, is shown to extend somewhat diagonally from southwest to northeast, indicating that the flow is not strictly meridional.

In addition to the observations from the two lidars, 22 dropsondes were deployed during the flight. Dropsondes provide an excellent source of comparison data set for the lidar wind and

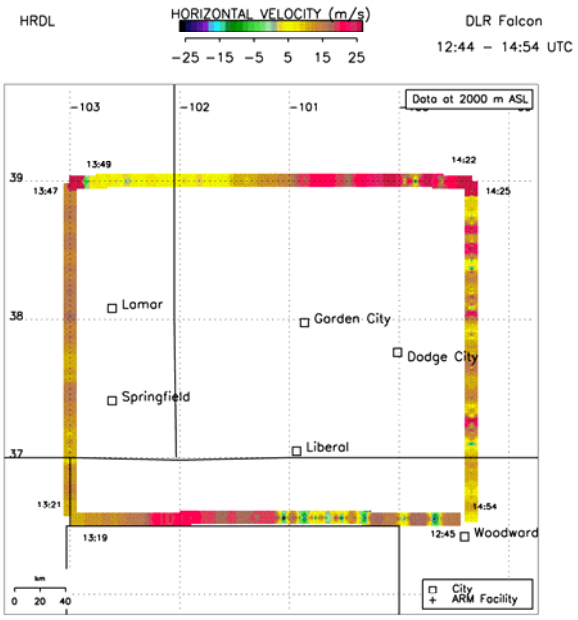

Figure 4: Flight track for June 9 LLJ case. Color indicates meridional wind speed at 2000 m AGL.

moisture measurements. Figure 5 shows an example of a lidar-dropsonde wind comparison taken at 14:32, just after the flight track turned to the south on the east side of the measurement box. For this comparison, the dropsonde data are resolved along the line-of-sight of the lidar (in this case measuring the westerly component) The lidar is seen to observe the sharp peak in the wind speed at 2 km, and accurately measure the winds to just above the surface up to flight altitude.

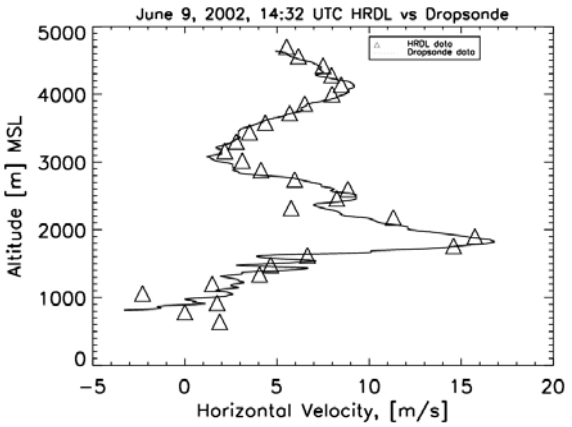

Figure 5: Comparison of lidar horizontal wind measurement with component of dropsonde wind computed along lidar line-of sight

Although data were taken on all legs of the flight track, instrument issues resulting primarily from intense heat in the cabin (cabin temperature approached 40^{O}) resulted in data dropouts during certain portions of the flight. The highest quality measurements from both instruments were on the northernmost west to east leg, which was flown between 13:50 and 14:24 UTC. This leg will be examined in detail in the rest of the paper.

Figure 6 shows the meridional component of the wind measured by HRDL along with the corresponding water vapor profile computed from the DIAL measurements for the northerly leg. Time corresponds to west to east distance; with the total horizontal extent of the plot corresponding to just over 285 km. Data in both cases have been processed at 150 m vertical resolution. The large dark area shown in the DIAL data at around 14:03 represents data loss resulting from laser instability. The measurements show similar structures, in particular a region of elevated water vapor and increased winds beginning near the surface on the west and gradually growing to a level approximately 2.5 km thick at the easternmost portion of the leg. Also note that the regions of highest winds and water vapor occur at roughly the same place along the track (just after 14:15), although water vapor peaks near the surface while winds are highest at about 2 km AGL.

Figure 7 shows the south-to-north flux of water vapor, computed by multiplying the wind speed by the water vapor concentration and reported in units of g m (kg s)$^{-1}$. A broad area of water vapor transport with values exceeding 200 and approaching 300 g m (kg s)$^{-1}$ and extending over about half the 285 km flight path can be seen.

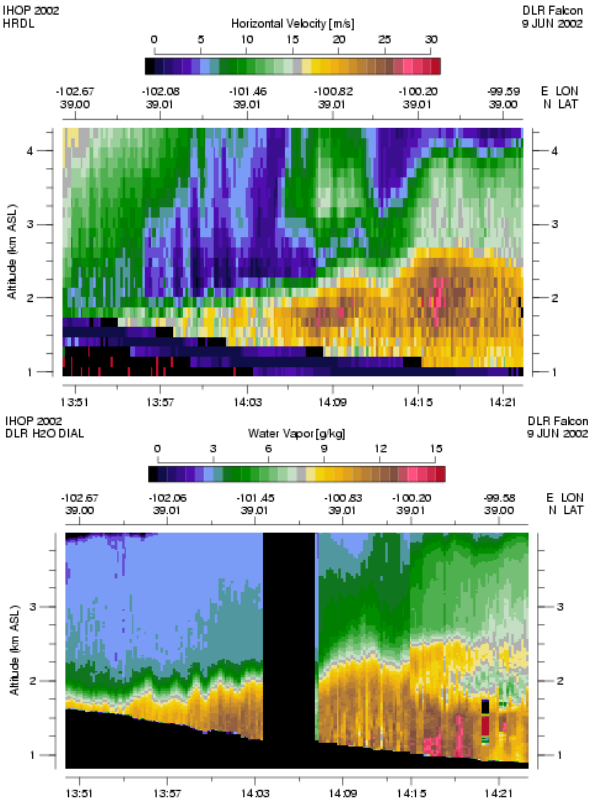

Figure 6: HRDL measurements of meridional wind speed (top) and DIAL water vapor concentration (bottom) computed along northern flight leg of Figure 4. Black area in the lower figure indicates missing data.

Most of the moisture in this region is transported in the layer extending from the surface to about 2.5 km.

Although the portion of the cross-section where significant water vapor transport exists is quite long (~140 km), examination of the flux levels as a function of distance along the flight leg reveals considerable structure. In Figure 8, which shows the flux value computed for each point along the flight path at a height of 2300 m, two distinct regions, or lobes, of high flux values are observed. Width of these lobes is on the order of 50-60 km. Also seen in Figure 7 are flux values computed from dropsondes deployed at several positions along the path. For this case, by chance, the dropsonde releases corresponded with local minima in the flux values. Thus, computation of fluxes based strictly on the dropsondes would have resulted in an underestimate of the true flux values. Figure 9 shows the total flux computed along the flight path for each height based on lidar and dropsonde measurements. It is seen that the dropsondes underestimated the flux by about 25%

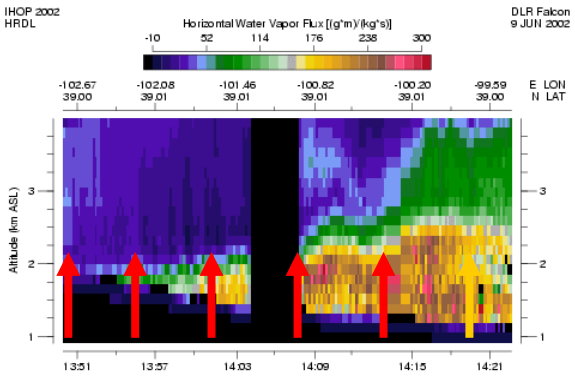

Figure 7: Moisture flux computed point by point from HRDL and DIAL measurements along northern west to east flight path. The total horizontal distance corresponds to about 285 km. Black area indicates missing data. Arrows indicate dropsonde releases.

over much of the profile. For this case, the dropsonde spacing was twice what would have been required to avoid aliasing and to adequately resolve the structure of the water vapor transport.

As noted earlier, the orientation of the jet was not completely meridional, as anticipated, but oriented at an angle of about 30 degrees from true north. Therefore, in only measuring a single component of the wind corresponding to the north south moisture transport, the lidar measurements are underestimating the true flux. A comparison of the zonal and meridional components of the moisture flux as a function of height computed from the dropsonde at 12:51 UTC was compared with the lidar measured flux profile. Although the meridional dropsonde and lidar measured fluxes agreed quite well, we observed that the zonal component of the flux was about half of the meridional flux, meaning that for this case the single component measurements significantly underestimated the total transport. Clearly both components of the wind and the flux need to be measured in future deployments to avoid errors .

4.0 SUMMARY

During IHOP we demonstrated the feasibility of co-deploying a DIAL and Doppler lidar on a single airborne platform and combining the measurements to estimate vertical (Kiemle et al, 2007) and horizontal flux of water vapor. Despite a somewhat crude setup, in which the return from the ground was used to correct for pointing errors, the method yielded good results, as evidenced in comparisons with dropsondes deployed along the flight track. The 1.5 km resolution lidar data revealed structure in the wind, moisture, and flux fields not observed by the dropsondes, which were deployed with a spacing of approximately 50 km.

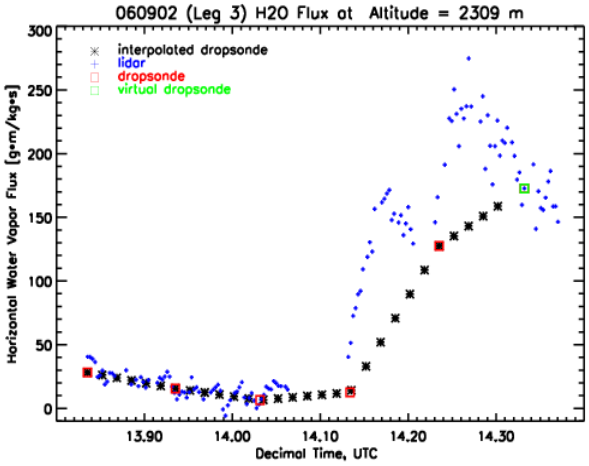

Figure 8: Comparison of lidar flux measurements with flux estimated from dropsondes (red squares). Crosses show interpolated dropsonde measurements. Green square is a "virtual dropsonde" corresponding to the lidar estimate

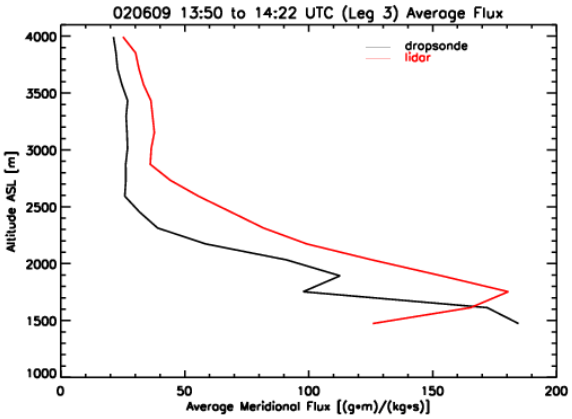

Figure 9: Comparison of meridional flux integrated over northerly leg from lidar measurements and from dropsondes.

Inability to resolve this structure meant that dropsonde-based estimate of total meridional moisture flux transported by the low level jet was biased low relative to the higher resolution lidar measurements.

5.0 REFERENCES

Ehret, G., K. P. Hoinka, J. Stein, A. Fix, C. Kiemle, and G. Poberaj, 1999: Low-stratospheric water vapor measured by an airborne DIAL. *J. Geophys. Res.,* **104,** 31 351–31 359
.

Grund, C. J., M. Banta, J. George, J. Howell, M. Post, R. Richter, and A. Weickmann, 2001: High-resolution Doppler lidar for boundary layer research. *J. Atmos. Oceanic Technol.,* **18,** 376–393.

Kiemle, C., W. A. Brewer, G. Ehret, R. M. Hardesty, A. Fix, C. Senff, M. Wirth, G. Pobaraj, and M. Lemone, 2007: Latent Heat Flux Profiles form Collocated Airborne Water Vapor and Wind Lidars during IHOP 2002, *J. Atmos. Ocean. Tech., 24, 627-639*